SCIENTIFIC REPORTS

OPEN

Optical thermometry based on level anticrossing in silicon carbide

A. N. Anisimov[1], D. Simin[2], V. A. Soltamov[1], S. P. Lebedev[1,3], P. G. Baranov[1], G. V. Astakhov[2] & V. Dyakonov[2,4]

Received: 06 June 2016
Accepted: 24 August 2016
Published: 14 September 2016

We report a giant thermal shift of 2.1 MHz/K related to the excited-state zero-field splitting in the silicon vacancy centers in 4H silicon carbide. It is obtained from the indirect observation of the optically detected magnetic resonance in the excited state using the ground state as an ancilla. Alternatively, relative variations of the zero-field splitting for small temperature differences can be detected without application of radiofrequency fields, by simply monitoring the photoluminescence intensity in the vicinity of the level anticrossing. This effect results in an all-optical thermometry technique with temperature sensitivity of 100 mK/Hz$^{1/2}$ for a detection volume of approximately 10^{-6} mm^3. In contrast, the zero-field splitting in the ground state does not reveal detectable temperature shift. Using these properties, an integrated magnetic field and temperature sensor can be implemented on the same center.

Temperature sensing with high spatial resolution may be helpful for mapping of biochemical processes inside living cells and monitoring of heat dissipation in electronic circuits[1–3]. Frequently used contact-less methods exploit temperature-dependent features either in Raman spectra of microfabricated chips[4,5] or in photoluminescence (PL) spectra of nanoprobes such as quantum dots[6], nanocrystals[7,8] and fluorescent proteins[9]. Typical temperature resolution of these methods is several hundreds of mK or lower.

Using quantum-mechanical properties of the nitrogen-vacancy (NV) in diamond, the temperature sensitivity better than $\delta T = 10$ mK/Hz$^{1/2}$ is achievable[3,10–12]. It is based on the moderate thermal shift $d\nu_0/dT = -74$ kHz/K[13,14] of the optically detected magnetic resonance (ODMR) frequency in the NV center ($\nu_0 = 2.87$ GHz at $T = 300$ K) and the use of the advanced readout protocols, particularly temperature-scanned ODMR[15] or thermal spin echo[10,11]. However, this method is not universally usable, because the application of high-power radiofrequency (RF) fields in the pulsed ODMR technique may alter the temperature at the probe during the measurement. Therefore, the realization of highly-sensitive and RF-free optical thermometry is of broad interest.

Our approach is based on the silicon vacancy (V_{Si}) centers in silicon carbide (SiC), demonstrating appealing properties for quantum sensing applications[16–18]. Particularly, the V_{Si} excited state[19,20] shows a giant thermal shift, exceeding 1 MHz/K[18]. Furthermore, these centers reveal an utterly long spin memory[21] and possess favorable absorption and PL in the near infrared spectral range[22], characterized by a deep tissue penetration. The concentration of the V_{Si} centers can be precisely controlled over many orders of magnitude down to single defect level[23,24] and they can be incorporated into SiC nanocrystals as well[25].

We perform proof-of-concept thermometry measurements using 4H-SiC crystals. The 4H-SiC sample under study was grown by the physical vapour transport method. Silicon vacancies were created by irradiation of the crystal with 2 MeV electrons with a fluence of 10^{18} cm^{-2}. The V_{Si} centers possess a half-integer spin state $S = 3/2$[26], which is split without external magnetic field in two Kramers degenerate spin sublevels $m_S = \pm 3/2$ and $m_S = \pm 1/2$. Here, we address the V_{Si}(V2) center[27] with the zero-field splitting (ZFS) in the ground state (GS) $2D_G = 70$ MHz [Fig. 1(a)]. The spin states are split further when an external magnetic field B is applied. The spin Hamiltonian of the V_{Si} center in the magnetic field has a complex form[20] and five RF-induced transitions are allowed: ν_1 ($-1/2 \leftrightarrow -3/2$), ν_2 ($+1/2 \leftrightarrow +3/2$), ν_3 ($+1/2 \leftrightarrow -3/2$), ν_4 ($-1/2 \leftrightarrow +3/2$) and ν_5 ($+1/2 \leftrightarrow -1/2$). In the ODMR experiments, we pump the V_{Si} centers into the $m_S = \pm 1/2$ state with a near infrared laser (785 nm or 808 nm with power in the range of several hundreds mW). To decrease the detection volume to approximately 10^{-6} mm^3, we use a near-infrared optimized objective with N.A. = 0.3. The PL is recorded in the spectral range

[1]Ioffe Physical-Technical Institute, 194021 St. Petersburg, Russia. [2]Experimental Physics VI, Julius-Maximilian University of Würzburg, 97074 Würzburg, Germany. [3]St. Petersburg National Research University of Information Technologies, Mechanics and Optics, 197101, St. Petersburg, Russia. [4]Bavarian Center for Applied Energy Research (ZAE Bayern), 97074 Würzburg, Germany. Correspondence and requests for materials should be addressed to G.V.A. (email: astakhov@physik.uni-wuerzburg.de) or V.D. (email: dyakonov@physik.uni-wuerzburg.de)

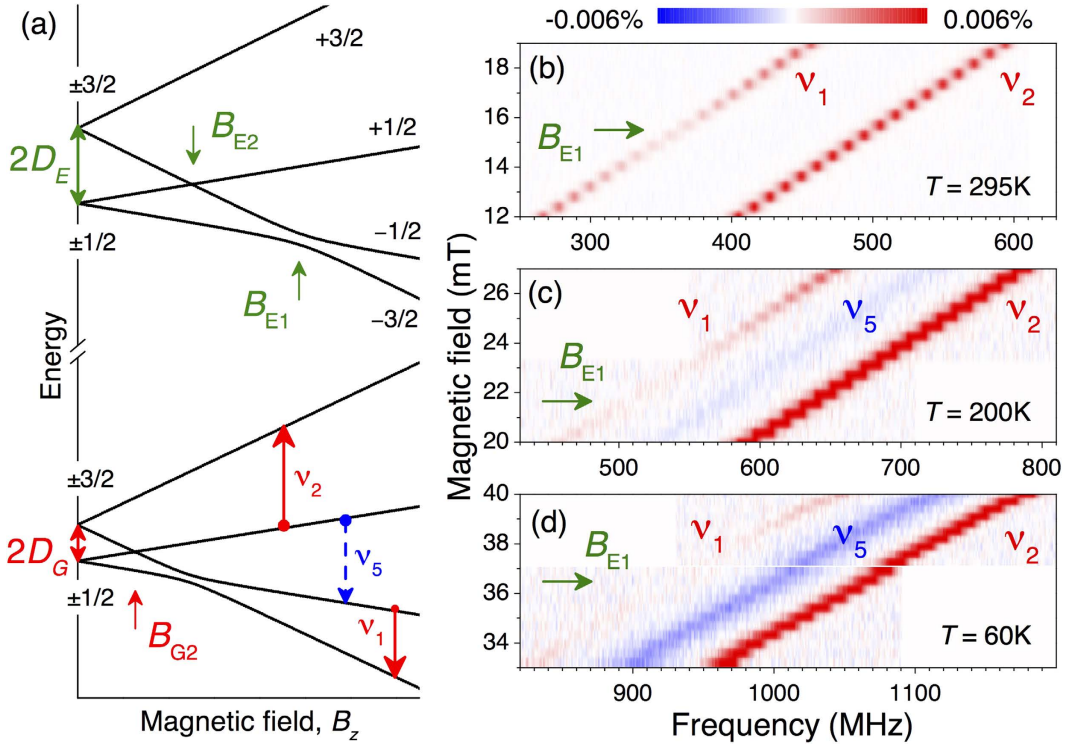

Figure 1. Indirect detection of the ES spin resonance in the V_{Si} center of 4H-SiC. (**a**) The GS and ES spin sublevels in the external magnetic field. The arrows labeled as ν_1, ν_2 and ν_5 indicate the RF driven transitions in the GS, detected in the experiment. (**b–d**) Magnetic field dependence of the V_{Si} ODMR spectra in the vicinity of the ESLAC-1, performed at different temperatures. The arrows indicate the magnetic field B_{E1}, at which the minimum ODMR contrast of the ν_1 transition is observed.

from 850 to 1000 nm, allowing optical readout of the V_{Si} spin state: it is higher for $m_S = \pm 3/2$. A detailed ODMR dependence on the magnetic field strength and orientation is presented elsewhere[20,28].

Due to the relatively short excited state (ES) lifetime of 6 ns in the V_{Si} center[22], the direct ODMR signal associated with the ES is weak. However, in the ES level anticrossing (LAC) between the $m_S = -1/2$ and $m_S = -3/2$ states (ESLAC-1) [magnetic field B_{E1} in Fig. 1(a)] the optical pumping cycle changes[29–32]. This results in a reduction of the ODMR contrast of the corresponding GS spin resonance[19,20].

Indeed, such a behavior is observed in our experiments. Figure 1(b) shows the magnetic field dependence of the ODMR spectrum in the vicinity of the ESLAC-1 at room temperature. The ν_1 and ν_2 lines shift linearly with magnetic field applied parallel to the symmetry axis ($B||c$) as $\nu_{1,2} = g_{||}\mu_B B/h \mp 2D_G$ for $g_{||}\mu_B B/h > 2D_G$ with $g_{||} = 2.0$ denoting the g-factor. The transition with $\Delta m_S = \pm 2$ are also allowed, but corresponding ν_3 and ν_4 lines appear at different frequencies and have lower ODMR contrast[20]. The ν_5 line is not resolved because of the same population of the $m_S = -1/2$ and $m_S = +1/2$ states under optical pumping at room temperature[26]. At $B_{E1} = 15.7$ mT, the ν_1 contrast drops to nearly zero and according to Fig. 1(a) the ES ZFS can be determined as $2D_E = g_{||}\mu_B B_{E1}/h$. Simultaneously, the GS ZFS is directly measured as $2D_G = (\nu_2 - \nu_1)/2$.

We repeat the above experiment at lower temperature $T = 200$ K [Fig. 1(c)]. One can clearly see that the magnetic field associated with the ESLAC-1 is shifted towards higher values $B_{E1} = 21.8$ mT, while the splitting between the ν_1 and ν_2 ODMR lines remains the same. In addition, another spin resonance with negative contrast becomes visible $\nu_5 = g_{||}\mu_B B/h$. We ascribe the appearance of the ν_5 line with lowering temperature with different transition rates to the $m_S = -1/2$ and $m_S = +1/2$ states. This may occur due to the either temperature-dependent interaction with phonons or some magnetic field misalignment, which in turn leads to the modification of the intersystem crossing as well as of the optical pumping cycle. The detailed analysis is beyond the scope of this work.

The tendency continues with lowering temperature down to $T = 60$ K [Fig. 1(d)]. Namely, we observe that the magnetic field associated with the ESLAC-1 is shifted to $B_{E1} = 36.5$ mT, indicating a further increase of D_E. The splitting between the ν_1 and ν_2 ODMR lines remains unchanged, suggesting D_G is nearly temperature independent. These findings are summarized in Fig. 2. The ES ZFS is well fitted to

$$2D_E(T) = 2D_E^{(0)} + \beta T, \tag{1}$$

with $2D_E^{(0)} = 1.06 \pm 0.02$ GHz denoting the ZFS in the limit $T \to 0$ and $\beta = -2.1 \pm 0.1$ MHz/K being the thermal shift. The latter is by more than one order of magnitude larger than that for the NV defect in diamond[13] and by a

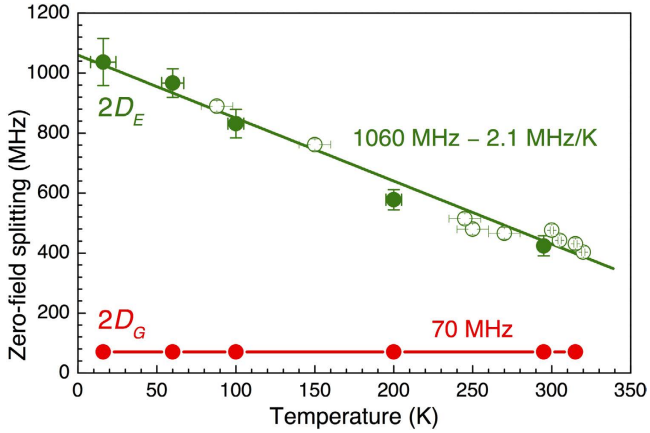

Figure 2. The GS ($2D_G$) and ES ($2D_E$) ZFS in the V_{Si} center of 4H-SiC as a function of temperature. Solid symbols are observed from the ODMR experiments of Fig. 1 and open symbols from the LAC experiments of Fig. 3. The line for $2D_E$ is a fit to Eq. (1). The line for $2D_G$ is to guide the eye.

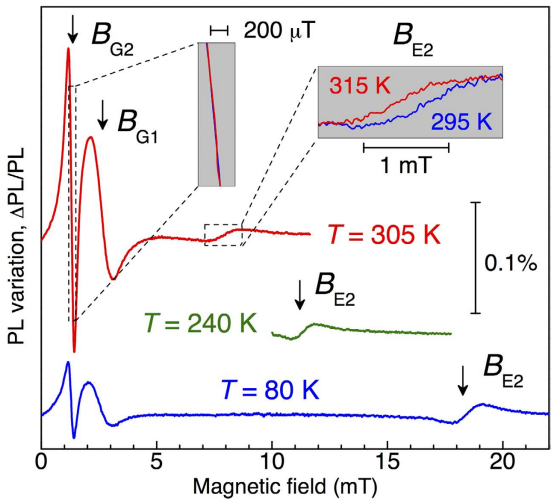

Figure 3. Lock-in detection of the PL variation ΔPL/PL (in-phase voltage U_X normalized to the *dc* photovoltage) as a function of the *dc* magnetic field *B*, recorded at different temperatures. ΔPL is caused by the application of an additional weak oscillating magnetic field. The arrows indicate the characteristic magnetic fields of different LACs. RF is not applied.

factor of two larger than previously reported for 6H-SiC[18]. In following, we use this giant thermal shift for all-optical temperature sensing.

The idea is to exploit the variation of the PL intensity in the vicinity of LAC, occurring even without RF fields. This method has been initially implemented for all-optical magnetometry in SiC[20], and later extended to the NV centers in diamond[33]. Figure 3 presents lock-in detection of the PL variation ΔPL/PL as a function of the *dc* magnetic field B_z, recorded at different temperatures. The modulation of PL is caused by the application of an additional weak oscillating magnetic field *B*, i.e., $B_z + \tilde{b}\cos\omega t$ with $\tilde{b} = 100$ mT and $\omega/2\pi = 0.33$ kHz. The sharp resonance at 1.25 mT corresponds to the LAC between the spin sublevels $m_S = -3/2$ and $m_S = +1/2$ ($\Delta m_S = 2$) in the GS, corresponding to GSLAC-2 in Fig. 1(a). A broader resonance at the double magnetic field of 2.5 mT relates to the LAC between the spin sublevels $m_S = -3/2$ and $m_S = -1/2$ ($\Delta m_S = 1$) , i.e., GSLAC-1. The magnetic fields corresponding to the LACs in the GS (B_{G1} and B_{G2}) are temperature independent, which is in agreement with our ODMR experiments of Fig. 1.

In addition to that, the experimental data of Fig. 3 reveal another resonance at the magnetic field B_{E2}. It corresponds to the LAC with $\Delta m_S = 2$ in the ES (ESLAC-2), as graphically explained in Fig. 1(a). Due to the strong reduction of the ES ZFS with growing temperature, this resonance shifts rapidly following Eq. (1) as $B_{E2} = hD_E(T)/(g_{\|}\mu_B)$. We recall that the lifetime in the ES is about 6 ns[22]. In order to observe ODMR signal associated with a spin state possessing such a short lifetime, one needs a RF field of about 2 mT. This alternating magnetic field, being in resonance with the spin transition, without strong impact on the temperature of the object under measurement is difficult to achieve.

We now discuss how small variations of the magnetic field ΔB and temperature ΔT can be measured. The in-phase lock-in voltage U_X at the bias field B_{G2} can be written as (left inset of Fig. 3)

$$U_X^{G2} = L_{11}\Delta B + L_{12}\Delta T\,. \tag{2}$$

Using calibration from our earlier experiments[20], we obtain $L_{11} = -39$ mV/mT. Because B_{G2} is temperature independent and the variation of the signal amplitude for $|\Delta T| < 10$ K is negligible, $L_{12} \approx 0$ mV/K is a good approximation. The linear dependence of Eq. (2) holds for $|\Delta B| < 100$ mT. The same can be written for U_X at the bias field B_{E2} (right inset of Fig. 3)

$$U_X^{E2} = L_{21}\Delta B + L_{22}\Delta T, \tag{3}$$

and we find $L_{21} = 1.8$ mV/mT and $L_{22} = 23$ mV/K. From the factors L_{ij}, it can be clearly seen that the magnetic field and temperature can be separately measured using GSLAC-2 and ESLAC-2. Particularly, the temperature sensing can be done in two steps. First, the bias field B_{G2} is applied and one measures U_X^{G2} to determine the actual magnetic field, accounting for ΔB in Eq. (3). Then, after applying B_{E2} and reading out U_X^{E2}, the magnetic noise can be excluded from the thermometry signal using

$$\Delta T = \frac{1}{L_{22}}\left(U_X^{E2} - \frac{L_{21}}{L_{11}}U_X^{G2}\right). \tag{4}$$

The dynamic temperature range of such thermometry is $|\Delta T| < 10$ K. A broad range thermometry can be realized (with lower sensitivity) by scanning the magnetic field from 5 mT to 20 mT and determining B_{E2}, which can be then converted to temperature using $D_E = g_{\|}\mu_B B_{\mathrm{E2}}/h$ in combination with Eq. (1).

We measure the in-phase and quadrature lock-in signals as a function of time to determine the upper limit of the noise level δU at a given modulation frequency (0.33 kHz). Then using the calibrated values for the L-matrix, we recalculate the noise level into the temperature sensitivity $\delta T = \delta U/L_{22}$. It is estimated to be $\delta T \approx 100$ mK/Hz$^{1/2}$ within a detection volume of approximately 10^{-6} mm^3. By improving the excitation/collection efficiency and increasing the PL intensity (the V_{Si} concentration), the temperature sensitivity better than $\delta T \approx 1$ mK/Hz$^{1/2}$ is feasible with a sensor volume of 1 mm^3. The suggested all-optical thermometry can be realized using various color centers in different SiC polytypes[34,35]. Furthermore, because color centers in SiC can be electrically driven[36] even on single defect level[37], an intriguing perspective is the implementation of a LAC-based thermometry with electrical readout using photoionization of the ES[38].

References

1. Yang, J.-M., Yang, H. & Lin, L. Quantum Dot Nano Thermometers Reveal Heterogeneous Local Thermogenesis in Living Cells. *ACS Nano* **5,** 5067–5071 (2011).
2. Yue, Y. & Wang, X. Nanoscale thermal probing. *Nano Reviews* **3,** 251 (2012).
3. Kucsko, G. *et al.* Nanometre-scale thermometry in a living cell. *Nature* **500,** 54–58 (2013).
4. Kim, S. H. *et al.* Micro-Raman thermometry for measuring the temperature distribution inside the microchannel of a polymerase chain reaction chip. *Journal of Micromechanics and Microengineering* **16,** 526–530 (2006).
5. Beechem, T., Graham, S., Kearney, S. P., Phinney, L. M. & Serrano, J. R. Invited Article: Simultaneous mapping of temperature and stress in microdevices using micro-Raman spectroscopy. *Review of Scientific Instruments* **78,** 061301 (2007).
6. Walker, G. W. *et al.* Quantum-dot optical temperature probes. *Applied Physics Letters* **83,** 3555 (2003).
7. Vetrone, F. *et al.* Temperature Sensing Using Fluorescent Nanothermometers. *ACS Nano* **4,** 3254–3258 (2010).
8. Plakhotnik, T., Doherty, M. W., Cole, J. H., Chapman, R. & Manson, N. B. All-Optical Thermometry and Thermal Properties of the Optically Detected Spin Resonances of the NV −Center in Nanodiamond. *Nano Letters* **14,** 4989–4996 (2014).
9. Donner, J. S., Thompson, S. A., Kreuzer, M. P., Baffou, G. & Quidant, R. Mapping Intracellular Temperature Using Green Fluorescent Protein. *Nano Letters* **12,** 2107–2111 (2012).
10. Toyli, D. M., de las Casas, C. F., Christle, D. J., Dobrovitski, V. V. & Awschalom, D. D. Fluorescence thermometry enhanced by the quantum coherence of single spins in diamond. *Proceedings of the National Academy of Sciences* **110,** 8417–8421 (2013).
11. Neumann, P. *et al.* High-Precision Nanoscale Temperature Sensing Using Single Defects in Diamond. *Nano Letters* **13,** 2738–2742 (2013).
12. Wang, J. *et al.* High-sensitivity temperature sensing using an implanted single nitrogen-vacancy center array in diamond. *Physical Review B* **91,** 155404 (2015).
13. Acosta, V. M. *et al.* Temperature Dependence of the Nitrogen-Vacancy Magnetic Resonance in Diamond. *Physical Review Letters* **104,** 070801 (2010).
14. Toyli, D. M. *et al.* Measurement and Control of Single Nitrogen-Vacancy Center Spins above 600 K. *Physical Review X* **2,** 031001 (2012).
15. Babunts, R. A. *et al.* Temperature-scanned magnetic resonance and the evidence of two-way transfer of a nitrogen nuclear spin hyperfine interaction in coupled NV-N pairs in diamond. *Journal of Experimental and Theoretical Physics Letters* **95,** 429–432 (2012).
16. Baranov, P. G. *et al.* Silicon vacancy in SiC as a promising quantum system for single-defect and single-photon spectroscopy. *Physical Review B* **83,** 125203 (2011).
17. Riedel, D. *et al.* Resonant Addressing and Manipulation of Silicon Vacancy Qubits in Silicon Carbide. *Physical Review Letters* **109,** 226402 (2012).
18. Kraus, H. *et al.* Magnetic field and temperature sensing with atomic-scale spin defects in silicon carbide. *Scientific Reports* **4,** 5303 (2014).
19. Carter, S. G., Soykal, Ö. O., Dev, P., Economou, S. E. & Glaser, E. R. Spin coherence and echo modulation of the silicon vacancy in 4H-SiC at room temperature. *Physical Review B* **92,** 161202 (2015).
20. Simin, D. *et al.* All-Optical dc Nanotesla Magnetometry Using Silicon Vacancy Fine Structure in Isotopically Purified Silicon Carbide. *Physical Review X* **6,** 031014 (2016).
21. Simin, D. *et al.* Long-lived quantum memory in silicon carbide with natural isotope abundance. *arXiv:1602.05775*.
22. Hain, T. C. *et al.* Excitation and recombination dynamics of vacancy-related spin centers in silicon carbide. *Journal of Applied Physics* **115,** 133508 (2014).
23. Widmann, M. *et al.* Coherent control of single spins in silicon carbide at room temperature. *Nature Materials* **14,** 164–168 (2015).

24. Fuchs, F. *et al.* Engineering near-infrared single-photon emitters with optically active spins in ultrapure silicon carbide. *Nature Communications* **6,** 7578 (2015).
25. Muzha, A. *et al.* Room-temperature near-infrared silicon carbide nanocrystalline emitters based on optically aligned spin defects. *Applied Physics Letters* **105,** 243112 (2014).
26. Kraus, H. *et al.* Room-temperature quantum microwave emitters based on spin defects in silicon carbide. *Nature Physics* **10,** 157–162 (2014).
27. Sörman, E. *et al.* Silicon vacancy related defect in 4H and 6H SiC. *Physical Review B* **61,** 2613–2620 (2000).
28. Simin, D. *et al.* High-Precision Angle-Resolved Magnetometry with Uniaxial Quantum Centers in Silicon Carbide. *Physical Review Applied* **4,** 014009 (2015).
29. van Oort, E. & Glasbeek, M. Fluorescence detected level-anticrossing and spin coherence of a localized triplet state in diamond. *Chemical Physics* **152,** 365–373 (1991).
30. Martin, J. P. D. *et al.* Spectral hole burning and Raman heterodyne signals associated with an avoided crossing in the NV centre in diamond. *Journal of Luminescence* **86,** 355–362 (2000).
31. Epstein, R. J., Mendoza, F. M., Kato, Y. K. & Awschalom, D. D. Anisotropic interactions of a single spin and dark-spin spectroscopy in diamond. *Nature Physics* **1,** 94–98 (2005).
32. Rogers, L. J., McMurtrie, R. L., Sellars, M. J. & Manson, N. B. Time-averaging within the excited state of the nitrogen-vacancy centre in diamond. *New Journal of Physics* **11,** 063007 (2009).
33. Wickenbrock, A. *et al.* Microwave-free magnetometry with nitrogen-vacancy centers in diamond. *arXiv:1606.03070.*
34. Falk, A. L. *et al.* Polytype control of spin qubits in silicon carbide. *Nature Communications* **4,** 1819 (2013).
35. Soltamov, V. A. *et al.* Optically Addressable Silicon Vacancy-Related Spin Centers in Rhombic Silicon Carbide with High Breakdown Characteristics and ENDOR Evidence of Their Structure. *Physical Review Letters* **115,** 247602 (2015).
36. Fuchs, F. *et al.* Silicon carbide light-emitting diode as a prospective room temperature source for single photons. *Scientific Reports* **3,** 1637 (2013).
37. Lohrmann, A. *et al.* Single-photon emitting diode in silicon carbide. *Nature Communications* **6,** 7783 (2015).
38. Bourgeois, E. *et al.* Photoelectric detection of electron spin resonance of nitrogen-vacancy centres in diamond. *Nature Communications* **6,** 8577 (2015).

Acknowledgements

A.N.A., V.A.S. and P.G.B. acknowledge support by the RSF Nr. 14-12-00859; the RFBR Nr. 14-02-91344; 16-02-00877. D.S. and G.V.A. acknowledge support by the BMBF under the ERA. Net RUS Plus project "DIABASE". V.D. acknowledges support by the DFG (DY 18/13-1). This publication was supported by the Open Access Publication Fund of the University of Wuerzburg.

Author Contributions

P.G.B., V.A.S., G.V.A. and D.S. conceived different parts of the experiments; A.N.A. and D.S. performed the experiments; S.P.L. provided the samples; G.V.A. wrote the manuscript; V.D. and P.G.B. supervised the project; all authors discussed the results.

Additional Information

Competing financial interests: The authors declare no competing financial interests.

How to cite this article: Anisimov, A. N. *et al.* Optical thermometry based on level anticrossing in silicon carbide. *Sci. Rep.* **6**, 33301; doi: 10.1038/srep33301 (2016).

This work is licensed under a Creative Commons Attribution 4.0 International License. The images or other third party material in this article are included in the article's Creative Commons license, unless indicated otherwise in the credit line; if the material is not included under the Creative Commons license, users will need to obtain permission from the license holder to reproduce the material. To view a copy of this license, visit http://creativecommons.org/licenses/by/4.0/

© The Author(s) 2016